A combination of methods for mapping heat and cool areas in past and current urban landscapes of Poitiers (France)

Axel Jame, Charlotte Noizat, Elie Morin, Hélène Paulhac, Yvonnick Guinard, Thomas Rodier, Romain Michenaud, Romain Pigeault, Jean-Louis Yengué, Thibaut Preux, et al.

Ecological Indicators 167 (2024) 112712

Contents lists available at ScienceDirect

Ecological Indicators

journal homepage: www.elsevier.com/locate/ecolind

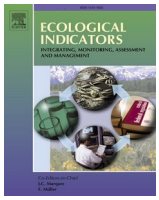

A combination of methods for mapping heat and cool areas in past and current urban landscapes of Poitiers (France)

Axel Jame [a,1], Charlotte Noizat [a,1], Elie Morin [b,1], Hélène Paulhac [a], Yvonnick Guinard [d], Thomas Rodier [d], Romain Michenaud [d], Romain Pigeault [a], Jean-Louis Yengué [c], Thibaut Preux [c], Dominique Royoux [c], Sophie Beltran-Bech [a,2], Nicolas Bech [a,2,*]

[a] Laboratory of Ecologie et Biologie des Interactions (EBI), UMR CNRS 7267, Poitiers University, Bâtiment B31, 3 Rue Jacques Fort, TSA 51106, 86073 Poitiers Cedex 9, France
[b] PictaMap, 2 avenue Galilée, 86360 Chasseneuil-du-poitou, France
[c] Laboratory of RURALITES, UR13823, Poitiers University, MSHS, Bâtiment A5, 5, rue Théodore-Lefebvre, TSA 21103, 86073 Poitiers Cedex 9, France
[d] Grand Poitiers Communauté Urbaine, 86000 Poitiers, France

ARTICLE INFO

Keywords:
Land use
Climate change
HMI modelling
Satellite data
Urban heat island

ABSTRACT

As a result of human activity, living organisms are faced with the consequences of both climate and landscape changes. These disturbances are particularly significant in urban environments, where an increase of areas are experiencing a rise in temperatures, creating urban heat islands (UHIs). Knowing the exact location of these areas and the factors involved in their formation would help to guide management measures aimed at reducing their impact. To locate heat and cool areas, this study uses, compares and combines satellite images (i.e. Land Surface Temperature = LST) and spatial modelling of an Heat Mitigation Index (i.e. HMI) in the urban landscape of Poitiers (France). We highlighted that the LST value differs according to the land use category. Indeed, while the highest temperatures were observed for high building density, moist tree vegetation and water areas are rather associated with the lowest temperatures. The results showed that the LST values correlate with the spatial modelling of HMI. Moreover, this correlation increases with the precision of the land cover (i.e. the number of land cover categories taken into account). While LST provides contextual information about heat, the HMI reflects the perceived heat according to the land cover. Thus, HMI modelling therefore showed that it appeared to be better suited to studying variations in highly heterogeneous landscapes such as urban landscapes and appear as a very interesting alternative to LST data when they are not available. Our approach is reinforced and corroborated by the installation of thermometers in the field. In addition, taking advantage of our improved HSI, we calculated the HSI and LST for two dates in 2020 and 1993. This demonstrated (i) the applicability of our method in the analysis of recent and past images and (ii) the contribution of our method to the study of the spatio-temporal evolution of heat and cool areas between two dates. The results of this study could help and guide future local urban planning in order to improve the mitigation and cooling potential of UHIs in the cities of tomorrow.

1. Introduction

Nearly 55 % of the world's human population live in urban areas and this rate could rise to 68 % by 2050 (United Nations, 2018). In France, 79.2 % of the population live in urban areas (INSEE, 2020)), and this phenomenon is expected to increase and contribute to urban sprawl and densification (Ramalho and Hobbs, 2012).

However, among human-induced alterations to land use, urbanisation causes the most significant and lasting change of natural landscapes on a global scale (Johnson and Munshi-South, 2017; Maxwell et al., 2016; Ramalho and Hobbs, 2012. Furthermore, the intensification of urbanisation, coupled with human activities, leads to an expansion of

* Corresponding author.
E-mail address: Nicolas.bech@univ-poitiers.fr (N. Bech).
[1] Co-first-authors have contributed equally.
[2] Co-last-authors have contributed equally.

https://doi.org/10.1016/j.ecolind.2024.112712
Received 16 February 2024; Received in revised form 4 October 2024; Accepted 4 October 2024
Available online 11 October 2024

artificial and mineralized surfaces at the expense of natural and semi-natural areas predominantly characterised by greenery (Halder et al., 2021; Yang et al., 2020). At a local level, this widespread artificialization can create artificial microclimates, causing a localised increase in temperature (Yang et al., 2020). In urban areas, surfaces such as tarmac roads, car parks, roofs, and walls contribute to heightened absorption of solar radiation, releasing stored energy in the form of heat. Although the presence of water could potentially mitigate this effect, the extensive sealing of soils rapidly drains surface water through run-off. As a result, heat is retained and added to the thermal impact generated by human activities such as industry and transport (Oke, 1976; Oke et al., 1991).

Cities therefore present areas where heat accumulates and can become trapped. These zones will therefore be characterised by a localised rise in temperature (compared with neighbouring rural areas) and are known as "urban heat islands" (i.e. UHI) (Taha, 2004). Depending on the study and on the studied area, UHI areas can be 5 to 15 °C warmer than surrounding areas (Santamouris et al., 2008; World Meteorological Organisation, 1984). For a long time, UHI were neglected in regional development plans but in the current context of global warming, they are at the centre of concerns as they can increase the energy demand in cities (Santamouris et al., 2008) and have a significant amount of repercussions on human health (Changnon et al., 1996; Hondula and Barnett, 2014). Furthermore, a study was published in 2022 governing the 3–30-300 rule. This rule is based on the premise that for people living in urban areas to have a better mental and physical health, they should be able to see at least 3 trees from every home, have 30 % tree cover in their neighbourhood and have access to an urban park within 300 m of their home (Konijnendijk, 2023; Nieuwenhuijsen et al., 2022). Indeed, local temperature rises can exacerbate heat waves, affecting the well-being and quality of life of the organisms occupying these areas (Elliott et al., 2020). This can induce a redistribution of organisms, including humans, who can develop thermoregulation problems (*e.g.* syncope, hyperthermia) and amplify chronic illnesses such as diabetes and cardiovascular diseases (Heaviside et al., 2017).

In the coming years, the frequency and intensity of heatwaves are expected to increase. (IPCC, 2023; Wouters et al., 2017). These projections, combined with the expected increase in urban dwellers to 68 % of the world's population by 2050 (United Nations, 2018), emphasise the need for rapid implementation of heat mitigation measures in cities to avoid or reduce heat stress. Accurate knowledge of the UHI location is essential for the effective implementation of appropriate measures. However, the typology of UHIs is not well defined because it depends on numerous environmental characteristics capable of influencing temperatures (*e.g.* latitude, altitude, types of landscapes, etc.). As a result, UHIs are not defined by a temperature threshold and can only be determined by comparing temperature differences between neighbouring areas.

The advancement of Earth monitoring campaigns has played a crucial role in acquiring high-resolution satellite images, offering valuable information for a variety of applications, including land planning, tracking pollution, and monitoring natural disasters. These applications are allowed by the numerous sensors integrated into satellites providing accurate, reliable and timely data recorded in different wavelengths of the electromagnetic spectrum. For instance, the Thermal-InfraRed (TIR) wavelengths are invisible to the human eye but provide an estimation of the temperature of the Earth's surface (Bonafoni et al., 2017; Mohammad and Goswami, 2021; Tomlinson et al., 2012). Besides, the estimated temperatures given by this wavelength match up significantly with the temperatures recorded between the ground and the treetops (Estoque and Murayama, 2017; Shi and Zhang, 2018). Although these images provide a very interesting estimate of ground temperature throughout the world, their coarse spatial resolution (i.e. 60–100 m) can limit their applications (Hu and Wendel, 2019; Mushore et al., 2017). For example, this can be the case in urban areas, where both the mosaic of microhabitats and the pronounced spatial heterogeneity can modify temperature at a very fine spatial scale (<10 m). Thus, in urban areas, other approaches are needed to accurately describe the spatial distribution of temperature variations and to locate UHI. Based on the land cover description, recently developed methods can describe the attenuation of heat by land cover categories such as vegetation (Bherwani et al., 2020; Bowler et al., 2010; Jones et al., 2022; Tieskens et al., 2022). Among these methods, the aproach implemented in the InVest program (Integrated Valuation of Ecosystem Services and Trade-offs) estimates urban cooling by calculating a heat mitigation index (i.e. HMI) using land cover description and ambient air of the study area (Sharp et al., 2020). To verify the credibility of the HMI, Zawadzka et al. (2021) investigated the correlation between HMI modelled using InVEST program and the empirical Land Surfaces Temperatures (i.e. LST) recorded by the Landsat program. The results showed that the HMI is highly correlated with the LST data, suggesting that it represents a good complement to the limitations of satellite imagery (such as spatial resolution or cloud cover) for identifying urban heat island zones. However, results also indicated that HMI is sensitive to cooling distance and resolutions of land cover maps used. Moreover, the authors only used seven land cover categories and did not test the influence of the number and diversity of land use categories on HMI modelling.

Herein, we tested the contribution of the number and diversity of land use categories to improve the HMI modelling. The correlation between the different HMI models and the empirical LST data were used as indicator of model improvement. Given that UHI effects are driven by factors such as building density, vegetation strata and urban surface albedo, we considered all of these variables to assess their impact on improving the calculation of HMI and enhancing its correlation with LST data. As a result, we hypothesised that adding all these land use categories to the calculation of the HMI will increase the correlation with the LST values. Low values of HMI are expected to correspond with high values of LST as well as for high values of HMI with low values of LST.

In other hand, taking advantage of our improved HMI, we calculated the HMI and LST for two dates in 2020 and 1993. This demonstrated (i) the applicability of our method in the analysis of recent and past images and (ii) the contribution of our methodology to the study of the spatio-temporal evolution of heat and cool areas between two dates.

While urban heat islands are on the increase in cities, this study aims to provide valuable information on the complex interaction between urban land use types, land surface temperature and their temporal dynamics, with potential implications for understanding urban development and environmental change.

2. Material and methods

2.1. Study area

The study area is located in the western Europe with a total area of 77 km^2 (from 65 to 144 m of elevation). Specifically, this study focuses on the city of Poitiers, France (wgs 84: 46.58◦ N, 0.34◦ E) which has a population of 90 033 people (INSEE 2020 census) and features a wide diversity of land covers resulting from a broad gradient of anthropic pressures (Fig. 1). While this study area is dominated by urbanisation, the land uses also include wetlands, agro-pastoral areas as well as an Urban Natural Park (along the river Le Clain). The long-established historic centre of Poitiers features a high urban density (housing and buildings), the peripheral areas are less dense but have experienced rapid urbanisation since the 1950 s (Morin, 2022).

The study area shows a predominantly oceanic climate and the weather data for the last 30 years shows mild temperatures (average annual temperature of 12.2 °C) and relatively abundant rainfall (average rainfall of 740 mm). All the climatic data required for this study is collected on the info climate website: https://www.infoclimat.fr for the Poitiers-Biard weather station (France).

This study aimed to investigate the heat and cool areas in recent (i.e. 2020) and past (i.e. 1993) landscapes, a period during which temperatures appear to have increased by 2 °C and precipitation to have

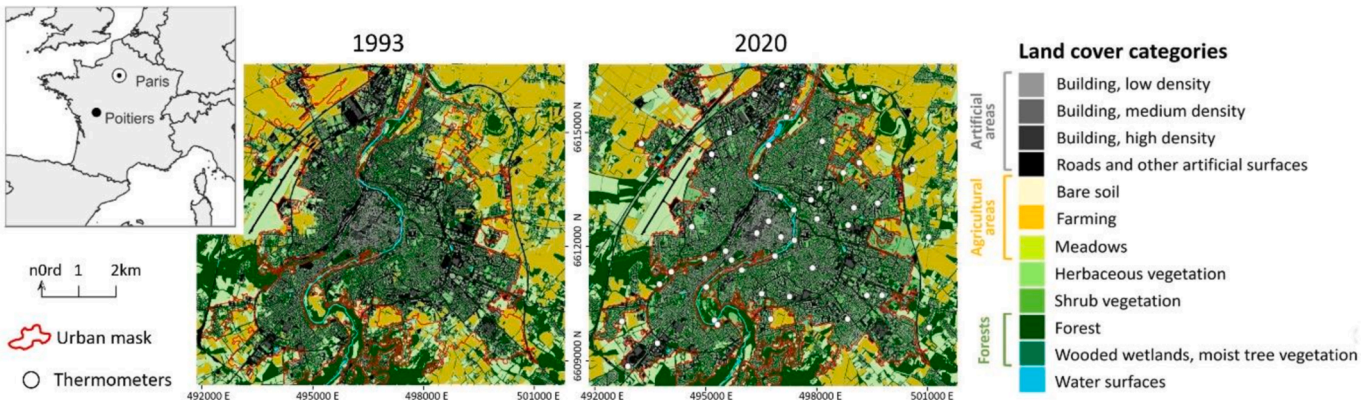

Fig. 1. Evolution of the land cover of the studied area between 1993 and 2020. The extent of this studied area corresponds to the square encompassing the urban fabric of Poitiers city determined by the 2020 French land use map (OSO) (Inglada et al., 2017).

decreased by around 200 mm/m^2 in the study area (Supplementary file 1). As mentioned above, the analyses in 2020 as well as in 1993 were intended to demonstrate (i) the suitability of our method to the analysis of past and recent images and (ii) the contribution of our method to the study of the spatio-temporal evolution of heat and cool zones between two dates.

2.2. Description of data used

2.2.1. Images recovered from satellite data

The satellites in the Landsat program (NASA and USGS) record and provide information reflected and emitted by the Earth in different wavelengths of the electromagnetic spectrum. From this program, we downloaded images of the study zone in 1993 (Landsat-5 Thematic Mapper (TM) scene acquired on 28 July 1993) and in 2020 (Landsat-8 Operational Land Imager (OLI) and Thermal Infrared Sensor (TIRS) scene acquired on 29 July 2020). These images were available on the USGS website (https://earthexplorer.usgs.gov/) (path 200, row28) and were free of clouds. July is expected to be a hot month with a wide temperature range. We resampled these images at 30 m.

2.2.2. Land cover maps

Land cover map of 1993: We used the existing land cover map developed in Morin et al. (2024). This map was built from existing institutionnal databases (i.e. BD TOPO vector database of the French National Geographic Institute (IGN)) that were modified using photo interpretation in order to describe built surfaces, water bodies and transport infrastructures in 1993 (spatial resolution, 0.5 m). Indeed, we removed features built after 1993 using the software QGis v.3.10. Trees, lawns and artificial areas were detected in urban context using geographic object-based classifications (GEOBIA) at a very high spatial resolution (0.5 m) from two orthophotos acquired on 28 July and 16 August 1993 (from IGN). The monotemporal classifications showed high global accuracy with an overall accuracy of 93.20 % and a Cohen's kappa of 0.897 for the northern image and an overall accuracy of 92.20 % and a Cohen's kappa of 0.881 for the southern image. See Morin et al.

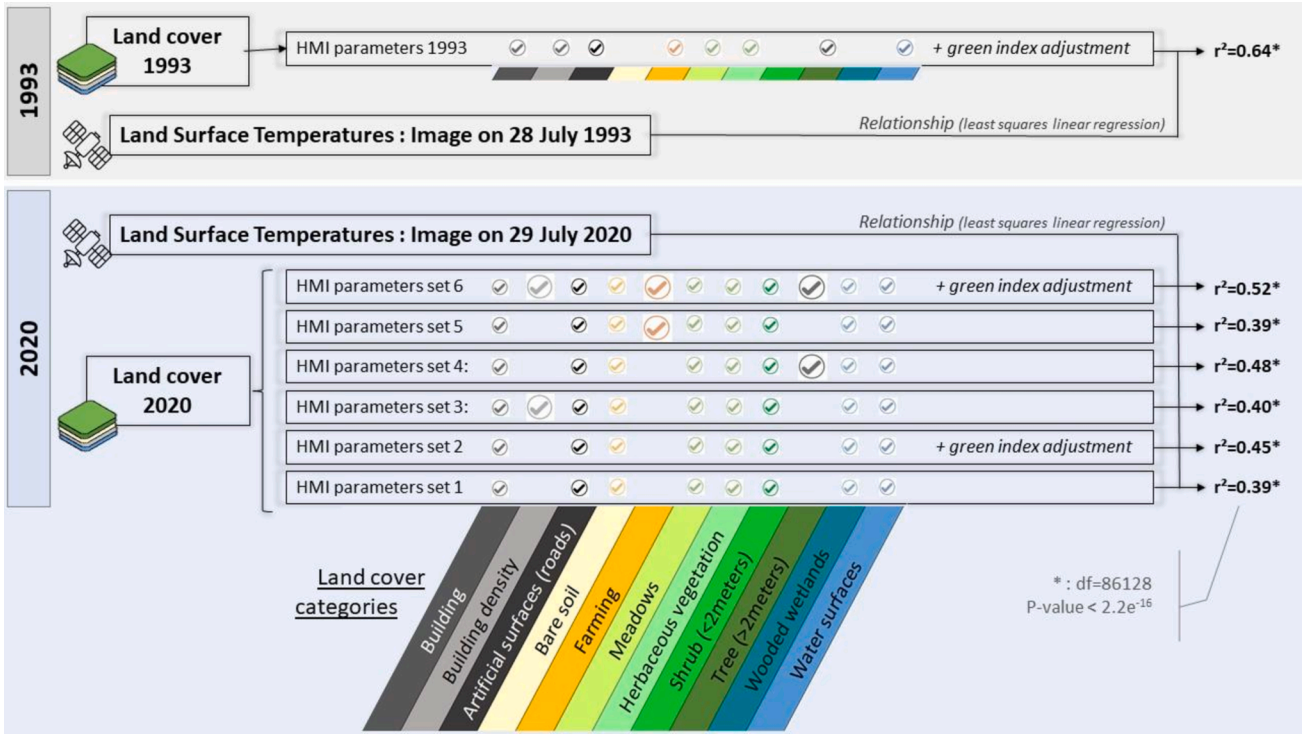

Fig. 2. Workflow and main steps of the whole research process.

(2024) for more details. Forests, meadows, croplands and urban areas were detected at a larger scale using a multitemporal classification using several Landsat-5 TM scenes. The classification showed an overall accuracy of 86.31 % and a Cohen's kappa of 0.832. Thus, we obtained a land cover map in 1993 at very high spatial resolution (i.e. 1 m per pixel) and including 9 land cover categories (Figs. 1 and 2), (supplementary file 2).

Land cover of 2020: As previously, we combined existing databases to characterise the land cover of the study zone in 2020 using QGis v.3.10 (Quantum GIS Development Team, 2019) (spatial resolution, 0.5 m). Specifically, we used the BD TOPO vector database of IGN to describe the distributions of water bodies, wooded wetlands, forests, transport infrastructures and buildings.

We characterised the density of buildings using a moving window analysis with a radius of 60 m to calculate the percentage of building pixels. The density was classified into three categories: low (0–33 %), medium (33–66 %) and high (66–100 %).

Furthermore, we obtained the agricultural plots (farming and meadows) by downloading the vector data Registre Parcellaire Graphique (RPG availaible at https://www.data.gouv.fr). Trees, lawns and urban areas were detected using a GEOBIA approach based on an orthophoto acquired on 19 July 2020. The classification showed good performances with an overall accuracy of 92.28 % and a Cohen's kappa of 0.897. We used a Digital Elevation Model (DEM) to classify tree vegetation into two strata: shrubs (1–2 m) and trees (>2 m). This DEM also allowed us to distinguish bare soil from bright buildings. We then obtained a land cover map in 2020 at very high spatial resolution (i.e. 1 m per pixel) and including 12 land cover categories (Figs. 1 and 2) (supplementary file 2).

2.3. Identification of heat and cool areas

2.3.1. Computing LST values from satellite images

We determined land surface temperatures (LST) from the reflectance emitted in TIR light from Landsat scenes recorded on 29 July 2020 and 28 July 1993. Primarily, we corrected these Landsat scenes with an atmospheric correction implemented in the Semi-automatic classification plugin of the software QGIS v.3.10 (Congedo, 2021). This correction is designed to compensate for the effects of absorption and scattering caused by the earth's atmosphere on the luminance measured by the optical sensor. Then, we estimated the ground surface temperatures using two steps. Firstly, the DN (Digital Number) values of the TIR data are converted into spectral radiance corresponding to the light intensity emitted by a surface in a given area. The second step consisted of converting the radiance into reflectance, which corresponds to the proportion of light reflected by the surface of a material (i.e. the ratio between the reflected luminous flux and the incident luminous flux). The reflectance is calculated by inverting the Planck radiation equation. Originally recorded in Kelvin degree, temperatures are then converted to Celius degree by subtracting 273.15. Full details of the calculations are available in Mueller et al. (2023) and on https://www.usgs.gov/.

2.3.2. Modelling the heat mitigation index

The procedure implemented in the InVEST (Integrated Valuation of Ecosystem Services and Trade-offs) program calculates values of the HMI and models the spatial distribution of its values across a study area. The HMI is based on the urban cooling model, recently developed by the Natural Capital Project (Sharp et al., 2020), which aims particularly to quantify the cooling effect and capacity of land cover categories, such as vegetation, in the city (Zawadzka et al., 2021). This index ranges from 0 (heat zones: UHI) to 1 (cool zones: UCI). We used InvEST to model the spatial distribution of HMI values within the studied area and according to land cover in 1993 and in 2020. Indeed, for each land cover category, the calculation of HMI values requires the determination of four biophysical variables (i.e. shade, crop coefficient Kc which determining the fraction of evapotranspiration evaporated by weighting water consumption according to the plant or type of plant cover (Zawadzka et al. 2021), albedo and green index) (supplementary file 1). Each biophysical variable was calculated using specific formulae described in detail in Zawadzka et al. (2021). Each biophysical can range from 0 to 1 depending on the land cover category, with the exception of Kc, which varies from 0 to 1.1 (InVEST user manual). In order to improve the calculation of HMI values, we propose to vary the green index coefficient for farming, meadows, herbaceous vegetation and water in order to better quantify and distinguish the cooling effect of these different land cover categories. Secondly, we propose to increase the thematic resolution (i.e. the number of land cover categories taken into account) of the land cover map with four supplementary categories (i.e. building density, shrub vegetation and bare soil) likely to influence and improve the calculation of HMI values. Thus, we carried out six different parameters sets (Fig. 2), (supplementary file 2).

- **The first parameters set** (i.e. parameters set 1) considers 8 land cover categories (Fig. 2). The other parameters sets represent different improved versions of this first parameter set.
- **The parameters set 2** proposes an adjustment of the green index which is usually a binary variable classified as 0 or 1. For this, we used the values of normalised difference vegetation index (NDVI) (Rouse et al., 1973), especially for farming, meadows, herbaceous vegetation and water surfaces. Indeed, these categories may provide a reduced cooling effect during heat waves due to drought. The NDVI has been widely used in remote sensing applications to identify and quantify vegetation health and density. Herein, we computed the NDVI from images recorded by Landsat-8 images on 29 july 2020. This index, which varies from −1 to 1, has been rescaled between 0 and 1 with the Orfeo Toolbox (OTB v.5.8) (Grizonnet et al., 2017) as other biophysical variables (Fig. 2).
- **The parameters set 3** distinguished three levels of building density, each with a different albedo and crop coefficients (Fig. 2).
- **The parameters set 4** considered shrub vegetation (< 2 m) with intermediate coefficients compared to herbaceous and tree vegetation (Fig. 2).
- **The parameters set 5** considered bare soil to distinguish albedo effect of bare soil from that of other artificial surfaces (Fig. 2).
- **The parameters set 6** compiled the different variables added in parameters sets 2–5 (Fig. 2).

See supplementary file 2 for more details about different parameters sets.

Concerning 1993, we computed the HMI values from the only land cover categories available for this period (n = 8). So, we did not consider the bare soils, the shrub vegetation and the wooded wetlands- moist tree vegetation (Fig. 2), (supplementary file 2).

Modelling of the spatial distribution of HMI values was carried out at a spatial resolution of 5 m in the study area.

The calculation of the HMI values also takes into account the potential annual evapotranspiration (ET0). This ET0 depends on both the meteorology and the topography of the studied area. First, we obtained the solar radiation using the r.sun.insoltime plugin implemented in the software QGis v.3.10 . This radiation was calculated as a function of topography (i.e. aspect, elevation and slope) and on the 15th day of each month, then averaged over the year. As mentioned previously, the climatic data were collected on the info climate website: https://www.infoclimat.fr for the Poitiers-Biard weather station. With the actual evapotranspiration (ETa), we then obtained by combining the radiation with the previous crop coefficient (Kc) specific to each land use category. In addition, we gave a higher ETa value for trees than for shrubs because trees can have a greater cooling effect than vegetation that is smaller. Following Zawadzka et al. (2021), shade was only provided by tree vegetation, simulating the sun at its zenith. We finally determined the maximum temperature mixing distance at 500 m, as recommended in the InVEST user manual. This distance represents the radius over which

air temperatures can be averaged, taking account of air mixing. We set the maximum cooling distance for vegetated areas at 100 m, as suggested by Zawadzka et al (2021). This distance corresponds to the perimeter for which large green spaces (i.e. > 2 ha) have a cooling effect beyond their boundaries. The other parameters we used to calculate the HMI are detailed in the InVEST user manual.

2.4. Relationships between the various studied parameters.

2.4.1. Installation of thermometers to validate the mapping approach

To validate our cartographic modelling (*in sillico*), we identified 25 heat zones and 25 cool zones where we installed 50 thermometers. To identify these different areas, we classified the HMI and LST values into four classes. Then, we selected the highest and lowest HMI and LST classes which overlapped to determine the most heatest and coolest areas.

The thermometers (LoraWan) were installed in July 2023 and recorded the temperature every 15 min. To determine whether the temperature was different between warmer and cooler zones, we focused on the hottest hours of the day (i.e., between noon and 3p.m.). We selected only the days for which at least 15 temperature sensors, within both warmer and cooler zones (i.e., 30 sensors in total), had recorded at least nine temperature measurements over the three hours period (on average one measurement every quarter of an hour).

The analysis was carried out on the average temperature per sensor over the focal period. A total of 109 days were included in the analysis. We used a mixed model procedure with a normal error structure and geographical site fitted as a random factor to test for an effect of site status (i.e., warmer or cooler zones) on temperature ('lme4' package, (Bates et al., 2015)). This analysis allowed us to control the spatial autocorrelation of data. Months were added as fixed factors into the model. As temperature could be expected to be a nonlinear function of month, the quadratic term month was added to assess whether it significantly improved the model fit. Maximal models, including all higher order interactions, were simplified by sequentially eliminating non-significant terms and interactions to establish a minimal model (Crawley, 2012). The significance of the explanatory variables was established using a likelihood ratio test (LRT, (Bolker, 2008). The significant LRT values given in the text are for the minimal model, whereas non-significant values correspond to those obtained before the deletion of the variable from the model. Statistical analyses were carried out using the R software (v.4.2.1) (R Core team, 2022). We then sampled and compared LST values in the warmer and cooler zones in 2020 and 1993. We used a Mann Whitney test to estimate the significance of these differences (Zar, 2010).

2.4.2. Relation between recorded temperatures, LST and HMI values

In order to assess the congruence between the LST data and HMI values computed using the six different parameters sets, we rescaled the spatial modelling of HMI values to 30 m. Consequently, we obtained the same spatial resolution for the LST and HMI maps, enabling them to be compared.

We then used the ordinary least squares linear regression to test the relationship between LST values and HMI values calculated from different sets of parameters. We carried out this procedure in 1993 and 2020. Statistical analyses were conducted using R software (v.4.2.1) (R Core team, 2022).

In addition, for each thermometer, we used a least squares linear regression to test the relationship between the mean temperature recorded by the different thermometers and the HMI values as well as LST values sampled on the grid where the thermometers were located. This would validate the different methods and give a proper comparison.

2.4.3. Influence of land cover on the surrounding temperature

To estimate the influence of the different land cover categories on temperatures, we calculated and averaged LST values for each land cover category. We then compared these values using a Kruskall-Wallis test followed by a Wilcoxon post-hoc test. We have not determined the influence of land use on the HMI values, as the calculation of these values is based in particular on the land use categories themselves. Statistical analyses were conducted using R software (v.4.2.1) (R Core team, 2022).

2.5. Spatio-temporal evolution of LST and HMI values between 1993 and 2020

To visualise the spatio-temporal evolution of both heat and cool zones between 1993 and 2020, we created, within the study area, a 60x60 meter grid to extract the mean values of LST and HMI (i.e. parameters set 1 – (Fig. 2), (supplementary file 2)). Then, to test the difference in the spatial distribution of heat and cool zones between the two dates, we carried out a pairwise comparison of the LST and HMI values between 1993 and 2020 using a Student's *t*-test. In addition, to visualise the spatio-temporal evolution of LST and HMI between the involved period, we subtracted the LST and HMI values calculating in 1993 and 2020 (i.e. HMI modelled using parameters set 3 – (Fig. 2), (supplementary file 2).

Parameter 3 offers two more land cover categories than the 1993 map. However, we believe that the analysis between the two dates is still possible, as these two categories (i.e. « bare soil » and « Wooded wetlands and moist tree vegetation ») represent very small areas in 2020, with 2.47 % and 0.34 % of the studied area respectively.

3. Results

3.1. Relation between temperature and land cover

Firstly, the temperature data, recorded by thermometers from 1 July 2023 to 1 June 2024, showed a lower average temperature in the zones identified as cooler than in the zones identified as heater (mean ± se, cooler zones = 15.86 ± 0.16; warmer zones: 16.43 ± 0.15). The temperature was strongly influenced by the month of the year (LRT = 3569.0, $p < 0.0001$, estimate = 7.18 CI95%: 6.99——7.37). Adding the quadratic term month2 significantly increases the model's fit (LRT = 3290.2, $p < 0.0001$). Indeed, the temperature follows an inverted bell curve, with temperatures falling in winter and rising in spring (Fig. 3). The status of the geographic site (i.e., cooler or heater zones) also had a significant influence on temperature (LRT = 7.8, p = 0.005, estimate = -0.49, CI95%: −0.825 − −0.154, Fig. 3). This suggested that the single Landsat image (recorded on 29 July 2020) that we used accurately reflected the overall climate trend of our study area (at least over the period recorded, ~one year) as well as the trend found in the LST data values (2020) between the heatest (i.e. mean 33.89 ± 1.05) and coolest zones (i.e. mean 28.21 ± 1.69) (p value < 0.0001). We don't have empirical data concerning temperature in 1993, but the heatest and coolest areas identified in 2020 are located in regions that also showed higher (i.e. mean 28.20 ± 1.64) and lower (i.e. mean 24.76 ± 1.56) LST data in 1993 (p-value < 0.0001).

3.2. Correlation between recorded temperature, LST and HMI values

As expected, the congruence between the two involved methods reveals HMI values negatively and significantly correlated with LST values suggesting that high temperatures result in low HMI values and lower temperatures are associated with high HMI values. The degree of correlation between these two variables depends on the parameters set used to calculate HMI values. Indeed, with the exception of the bare soil category (i.e. parameters set 5), the addition of land cover categories as well as the adjustment of the green index, for instance, increase and improve the correlation between the HMI and the LST values (Fig. 2), (supplementary file 2). In 1993, HMI and LST values were also significantly correlated (estimate = -8,0322, IC95% [-9.4212; −6,6431], t =

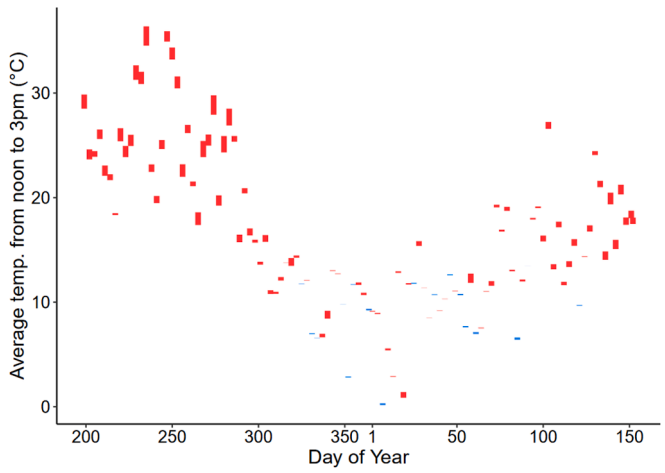

Fig. 3. Variation in temperature differences between cooler and heatest zones recorded over one year. The upper limit of each blue or red segment corresponds to the highest average temperature measured on a focal day, while the lower limit corresponds to the lowest average temperature measured. If the segment is red, the areas mapped as warmer are indeed warmer than the areas mapped as colder; if it is blue, the areas mapped as colder are warmer than the areas mapped as heater. The longer the segment, the greater the temperature difference between warmer and cooler areas. The first day of the temperature survey was 07–14-2023, i.e. day 195 of the year 2023. The study ended on 2024–06-01, i.e. day 153 of the year 2024.

-244.73, df = 86128, p-value < 0.01; adjusted R^2 = 0.64).

Moreover, results showed that the mean temperature recorded by thermometers was significantly correlated with HMI values (estimate = -0.8929, IC95%[-1.457; −0.329], t = -3.218; p = 0.002833; adjusted R^2 = 0.211) and with LST values (estimate = 0.07261, IC95%[0.005; 0.140], t = 2,195; p = 0.03507; adjusted R^2 = 0.09838) recorded on the grid where the thermometers were located.

3.3. Influence of land cover on temperature

LST values differ according to the land use category (Kruskal-Wallis chi^2 = 5741.8, df = 12, p-value < 0.01). LST values are significantly higher in artificial areas than near agricultural ones (p-value < 0.01), forests (p-value < 0.01) and water areas (p-value < 2e-16). The highest temperatures were observed for high building density (T = 34.7 °C) and increased significantly as a function of this variable. Moist tree vegetation and water areas are associated with the lowest temperatures (Fig. 4).

3.4. Spatio-temporal evolution of LST and HMI between 1993 and 2020

LST values recorded in 1993 and 2020 revealed differences. Indeed, the average LST value is significantly different between these two periods with 27 °C +/- 1.6 °C in 1993 and 32 +/- 2 °C in 2020 (t = -666.18, df = 86129, p-value < 0.01) (Fig. 4). Specifically, very high LST values (>36.6 °C) are over-represented in 2020 compared to 1993 while very low LST values (<23.4 °C) are almost absent in 2020 (Fig. 5). For information, the largest increases are observable on the outskirts of the city in large artificial areas (*e.g.*, commercial areas). Conversely, LST values decreased slightly in the northwest of the study area where the agricultural areas are located.

Subtracting the HMI values between 1993 and 2020 showed spatial variation over the period (Fig. 4). Specifically, the average HMI is significantly different between the two years with an average value of 0.29 +/- 0.19 in 1993 and 0.30 +/- 0.19 in 2020 (t = –23.769, df = 86129, p-value < 0.01) (Table 1).

Between these two periods, significant changes in land use between 1993 and 2020 could partly explain the recorded temperature differences. Cultivated land (−10 %) and grassland (−2%) decreased, while herbaceous vegetation and trees inside the city (9 %) increased. Indeed, it seems that the new residential neighbourhoods have replaced agricultural areas, but they include gardens with trees and lawns, as the results have shown an increase in low-density buildings (2 %) as well as herbaceous vegetation and trees within the city (9 %). The urbanised areas have expanded, particularly on the outskirts of the city, in the large shopping areas, where we have also recorded an increase in LST between 1993 and 2020 (Table 2).

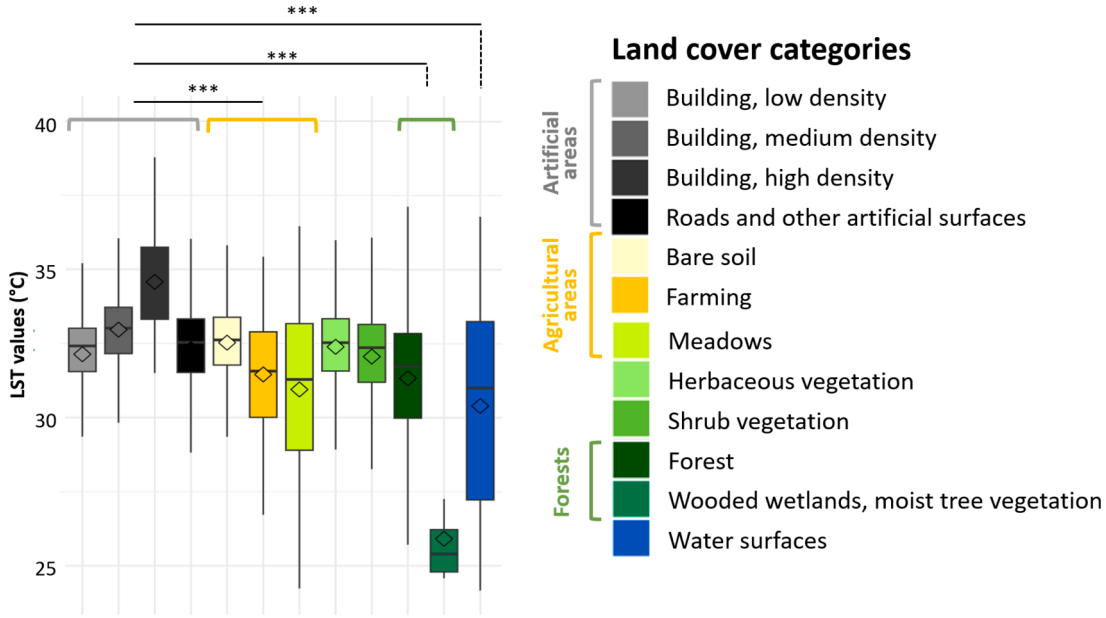

Fig. 4. LST values for each land cover category. The diamond represents the mean and the bold black bar the median. According to the Kruskall-Wallis test, followed by a Wilcoxon post-hoc test, LST values are significantly higher near artificial areas than agricultural ones (p-value < 0.01), forests (p-value < 0.01) and water areas (p-value < 0.01).

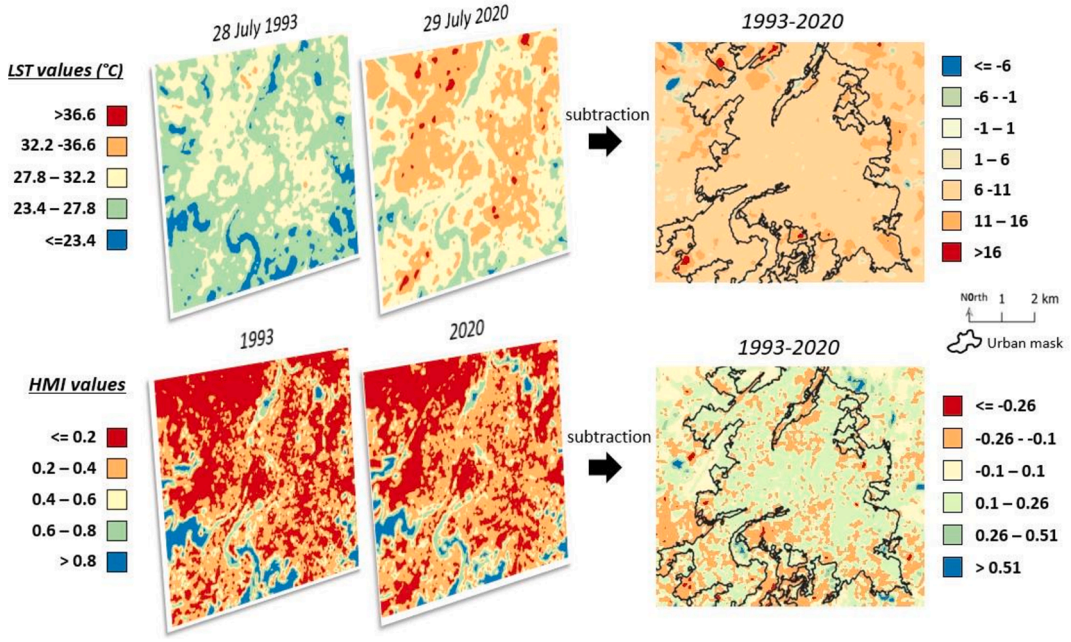

Fig. 5. Spatio-temporal evolution of LST (A) and HMI (B) values between 1993 and 2020 in the studied area.

Table 1
Mean, minimum and maximum values of HMI and LST in 1993 and 2020.

Values	1993		2020	
	HMI	LST	HMI	LST
Mean +/- SD	0.29 +/- 0.19	27 +/- 1.6 °C	0.30 +/- 0.19	32 +/- 2 °C
Minimum	0,04	19 °C	0,05	23 °C
Maximum	0,96	36 °C	0,95	40 °C

Table 2
Change in the surface area of different land use categories between 1993 and 2020.

Land cover categories		Area (km2) 1993	Area (km2) 2020	Changes (%)
Building	Building, low density	3.53	5.02	1.76
	Building, medium density	2.14	2.69	0.65
	Building, high density	0.64	0.81	0.2
Roads and other artificial surfaces		13.77	14.56	0.93
Farming		22.78	14.11	−10.23
Meadows		11.69	9.92	−2.09
Herbaceous vegetation		5.37	11.51	7.25
Shrub and trees		24.13	25.29	1.37
Water surfaces		0.64	0.78	0.17

4. Discussion

As a result of human activities, living organisms are faced with the consequences of both climate and landscape changes. These disruptions are particularly significant in urban environments, where 68 % of the human population is expected to live in 2050. Focused on the city of Poitiers, this study compares and combines two methods allowing (i) locating heat areas and (ii) to highlight the spatio-temporal evolution of these heat areas between 1993 and 2020.

4.1. Improving the heat mitigation index

As highlighted by Zawadzka et al. (2021), Our results show that the HMI values, provided by the InVEST program, are significantly correlated with the LST values when compared at 30 m spatial resolution. Even though explained variation did not exceed 51 % in our models for 2020, they reached 64 % in 1993. However, in 2020, we improved the correlation between HMI and LST values by modifying i) the green index based on the NDVI, ii) the building density, iii) the bright surfaces and iv) by differentiated vegetation strata. Based on the results, the most important parameters capable of improving the correlation seemed to be the green index adjustment and the consideration of the different vegetation strata. Whereas Zawadzka et al. (2021) set the green index at 1, we demonstrated that modifying this parameter based on the NDVI was useful. This parameter could be adapted according to vegetation stress scenarios and the specific vegetation types found in each study area around the world (Wloczyk et al., 2011). Close attention must also be paid to the accuracy of classifications made to detect urban vegetation. As vegetation is the main parameter in HMI modelling, classifications must be as accurate as possible to correctly represent urban heat islands. In addition, we observed that differentiating shrubs from trees strongly increases the correlation between HMI and LST values. 3D information is not often available, leading to produce land cover maps with only two vegetation strata: herbaceous and tree vegetation – shrubs are generally assimilated to the tree vegetation (Morin et al., 2022; Puissant et al., 2014). The urban cool areas, especially the shadow areas, tend to be overrepresented when such maps are used to model HMI leading to a lower correlation between HMI and LST. Here we show the importance of taking shrubs into account when calculating the HMI.

Interestingly, building density and bright surfaces (i.e. bare soil) did not enhance the strength of relationship between HMI and LST. Bright surfaces did not represent a large proportion of the study area which could explain this result. Concurrently, taking into account the density of the building mainly modified the values of the albedo and the crop coefficient, but these modifications remained relatively low compared with the values implemented in the default parameter set 1.

Numerous factors can affect the relationship between HMI and LST. For example, we only used a single LST image acquired on a warm summer morning. It would have been interesting to be able to use an image later in the day or during a heat wave, when surface temperatures

are higher, in order to potentially obtain a more significant correlation. Similarly, the use of several different dates for recording the LST would have enabled us to obtain a more accurate spatial variation in temperatures . Unfortunately, we did not have the opportunity to obtain more images due to excessive cloud cover on a large number of dates, which distorted the temperature data obtained using satellite sensors. A notable difference between LST and HMI values is spatial resolution. Indeed, LST are recorded at 30 m per pixel, whereas we have estimated HMI values at 5 m per pixel (corresponding to the spatial resolution of the available land use map in our studied area). HMI modelling calculations therefore seem to be better suited to studying variations in highly heterogeneous landscapes such as urban landscapes and appear as a very interesting alternative to LST data when they are not available. It should be noted that InVEST outputs also provide an estimate of ambient air temperature that can be modulated according to the climatic data. For example, Bosch et al. (2021) showed that the air temperature observations from monitoring stations better estimated air ambient temperature than spatial regression model using satellite data (Bosch et al., 2021). One of the strengths of the Urban Cooling Model implemented in the InVEST program is that it's not a black-box and all parameters can be adjusted. Consequently, we can adjust these parameters according to information available on the studied area. Herein, we modified the number of land cover categories and we adjusted the green coefficient (using NDVI) to enhance the calculation of HMI values. More investigations could propose integrating, for example, the shadows created by buildings (and therefore solar irradiance) which can influence land surface temperature (Freitas et al., 2015). However, the calculation of HMI values can also be improved by taking into account solar irradiation whose accuracy can be enhanced using models including beam, diffuse and reflected irradiance. Based on the Stefan-Boltzmann Law, describing the power radiated from a black body in terms of its temperature, such a model allows to estimate land surface temperature (Hofierka et al., 2020) which can be reinvested in the InVEST calculations. Even though this approach is very accurate, it does not consider air flow or the cooling distance capacity of large vegetation or water areas (Broadbent et al., 2018; Motazedian et al., 2020). Each approach has its strengths and weaknesses: methods that are exceptionally accurate can also be time-consuming and energy-consuming, these methods needing strong expertise are not applicable over a large study area (Bherwani et al., 2020; Freitas et al., 2015). As a result, the InVEST Urban Cool model represents a good compromise between accurate process modelling, the skills required, input data, and time/energy consumption.

4.2. Spatio-temporal evolution of temperatures and heat areas between 1993 and 2020

Although it is difficult to compare the absolute temperatures between 1993 and 2020 using only two snapshot satellite images, LST values recorded for the two dates suggested a rise of temperature which is in phase with global meteorological data. In concert with this, the study area also shows urban sprawl, characterised by an increase in artificialized areas (Table 2), which seems to increase local temperatures. These results are in line with previous studies showing that variations in land use can amplify the effect of heat zones (Liu et al., 2019; Ranagalage et al., 2017). Moreover, during the studied period, meteorological data recorded an annual increase in mean temperatures of around 2 °C as well as a decrease in precipitation in our study area. It is noted that the year 2020 was particularly warm (probably favoured by the onset of the Niña effect) compared to the year 1993 which was rather cold compared to previous and following years (supplementary file 1). This could explain, in part, the increase in July LST between these two dates (Table 1) since the air temperature varies with the land surface temperature (Shi and Zhang, 2018). However, even though we are only quoting the main weather trends over the period, it is difficult to conclude on the temporal changes in weather as we have only used two snapshot satellite images. We would need to use more satellite images to show the average temperature level and more time points to show the trend over the last 30 years. The difficulty and one of the limits of this method is therefore the availability of data, particularly in ancient historical periods due to the evolution of technologies over time and the availability of archival data.

It is difficult to estimate the spatial and temporal evolution of heat and cool areas as the LST values amplitudes between the two dates 1993 and 2020 are too different and the maximum LST value recorded in 1993 remains lower than that recorded in 2020. Based on this LST values increase over the studied period, it now seems important to estimate how this rise in temperature will impact humans. These estimates can be approximated using the HMI index.

The HMI values clearly reveal spatio-temporal changes of heat and cool zones between 1993 and 2020. These modifications are likely the result of land use changes during the studied period as we observed an increase in HMI values on the outskirts of the study area, where new commercial areas and buildings appear during the studied period. However, while artificial areas have increased on the overall scale of the study area, their proportion has not really changed in the city centre where we observe an increase of 7 % and 1 % in grassy areas and tree areas respectively. This can explain why we observe an increase of the HMI values in the centre of the study area. In addition, the HMI values calculated in 2020 also benefit from the planting carried out in 1993, which has expanded.

The spatial distribution of HMI values is very important for locating the cool areas that provide refuge for city dwellers as well as for biodiversity. According to our results, high HMI values are often associated with vegetation that also promotes the well-being of city dwellers (Cox et al. 2017, Luck et al. 2011, Nieuwenhuijsen et al., 2022). Specifically, this well-being of city dwellers seems to depend on the presence of at least three visible trees from their homes, a 30 % tree cover in the surrounding neighbourhood, and proximity to an urban park or forest within a 300-meter radius of their residences (Konijnendijk, 2023; Nieuwenhuijsen et al., 2022). In concert with this study, this confirms the importance of both thematic and spatial resolutions in cartography, especially in highly heterogeneous landscapes such as urban ones.

4.3. Implication in land policy and management

Firstly, it is imperative to prioritise the management of urban surface temperature, as it can be effectively controlled through strategic interventions. Additionally and in line with our results, addressing heat areas concerns requires a shift in perspective, recognizing that UHI effects extend beyond cityscapes alone (Onačillová and Gallay, 2018) and can include industrial and commercial areas. The calculation of HMI values considers four biophysical variables (i.e. shade, crop coefficient, albedo and green index) characterising each land component. These biophysical variables could provide a basis for land managers' actions in the field. Indeed, if we want to avoid heat areas in human-dominated landscapes, management strategies should incorporate nature-based solutions (Jones et al., 2022; Norton et al., 2015). For instance, it would be interesting to favour shade and the cooling effect of vegetation by promoting the planting of trees, shrubs, or even herbaceous vegetation (Elliott et al., 2020; Konijnendijk, 2023). Also, these green spaces serve as vital cooling agents, providing respite from elevated temperatures and improving overall environmental quality. By integrating these recommendations into urban planning and development practices, cities can effectively combat heat areas and create healthier, more resilient urban environments for present and future generations. Moreover, preserving semi-natural habitats such as wetlands and forests at the landscape scale is essential for maintaining ecological balance and enhancing the cooling influence of natural elements like rivers and forests. For building, it would be preferable to use suitable urban materials with high solar reflectance, thermal emissivity, and heat capacity to minimise heat absorption and reduce surface temperatures. In

addition, when constructing new buildings, it is important to take into account fluctuations in wind speed and air flow, which play an important role in heat reduction (Kim and Baik, 2005, 2002). Although these general suggestions (i.e. promoting vegetation and using environmentally friendly construction materials) seem effective in combating temperature effects, their implementation requires, beforehand, the precise location of vulnerable and at-risk areas. However, our results indicated that to effectively locate these vulnerable areas, it is crucial to use a highly accurate land cover map with a large number and diversity of land cover categories. Thus, attention should be paid to cartographic modelling based on low-quality land cover maps, which can lead to inaccurate land-use planning conclusions.

5. Conclusion

In this study, we calculated HMI values from different parameters sets and examined their correlation with LST derived from Landsat imagery. The improvement in the HMI has resulted in an improvement in thematic resolution. For exemple, HMI values correlate better with LST values when the density of buildings and the distinction between grasses, shrub and tree strata are taken into account.

We calculated the LST and HMI values for 2020 and 1993 in order to compare the spatio-temporal evolution of both heat and cool areas. Even if more satellite images should be used to show the average level, and more time points are needed to show the trend of the near 30 years, the results indicated a substantial increase in LST between 1993 and 2020 – in accordance with global meteorological data. The advantage of the HMI calculation lies in its potential to reflect temperature variations at a very fine scale, providing a deeper understanding of critical areas for both human and biodiversity considerations. Both approaches complement each other, offering insights into urban heat and cool islands at different scales. While LST provides contextual information about heat, the HMI values reflect the perceived heat experienced by living organisms, considering factors such as shaded areas.

In the context of climate change and increasing land urbanisation, these dual approaches emerge as highly relevant for effective land planning and predicting the impact of various scenarios. They offer valuable tools for finding optimal solutions to urban heat management and contribute to informed decision-making. As we navigate the challenges posed by climate change and urban expansion, integrating both LST and HMI provides a comprehensive understanding necessary for sustainable urban development.

CRediT authorship contribution statement

Axel Jame: Writing – review & editing, Writing – original draft, Visualization, Validation, Software, Methodology, Investigation, Formal analysis, Data curation, Conceptualization. **Charlotte Noizat:** Writing – review & editing, Writing – original draft, Visualization, Validation, Software, Methodology, Formal analysis, Data curation, Conceptualization. **Elie Morin:** Writing – review & editing, Writing – original draft, Visualization, Validation, Software, Methodology, Investigation, Formal analysis, Data curation, Conceptualization. **Hélène Paulhac:** Writing – review & editing, Validation. **Yvonnick Guinard:** Writing – review & editing, Validation. **Thomas Rodier:** Writing – review & editing, Validation. **Romain Michenaud:** Writing – review & editing, Validation. **Romain Pigeault:** Writing – review & editing, Validation. **Jean-Louis Yengué:** Writing – review & editing, Validation. **Thibaut Preux:** Writing – review & editing, Validation. **Dominique Royoux:** Writing – review & editing, Validation. **Sophie Beltran-Bech:** Writing – review & editing, Writing – original draft, Validation, Supervision, Project administration, Methodology, Funding acquisition, Conceptualization. **Nicolas Bech:** Writing – review & editing, Validation, Supervision, Project administration, Methodology, Funding acquisition, Conceptualization.

Declaration of competing interest

The authors declare that they have no known competing financial interests or personal relationships that could have appeared to influence the work reported in this paper.

Data availability

The authors do not have permission to share data.

Acknowledgements

This work was supported by Grand Poitiers Communauté Urbaine, the Nouvelle Aquitaine Region, the University of Poitiers as well as RURALITES and EBI Laboratories. We also thank the Agence Nationale de la Recherche, France (Grant No. ANR-21-CE32-0002-01 [RECODE] to N.B.), the Office Français de la Biodiversité, France, the intramural Funds from the University of Poitiers (UP-Squared: *INOVIE* and ERI: ONE CITY), the European Regional Development Fund (FEDER), the Chaire Biodiversité of the University of Poitiers, France and finally, the intramural Funds from the Centre National de la Recherche Scientifique, France (CNRS). We would like to thank the environmental associations: LPO and Vienne Nature for their important contribution to this work as well as Jean Peccoud for his help in statistics. Finally, we would particularly like to thank Thulilé Gaignerot for editing the manuscript.

Appendix A. Supplementary data

Supplementary data to this article can be found online at https://doi.org/10.1016/j.ecolind.2024.112712.

References

Bates, D., Mächler, M., Bolker, B., Walker, S., 2015. Fitting linear mixed-effects models using lme4. J. Stat. Softw. 67, 1–48. https://doi.org/10.18637/jss.v067.i01.

Bherwani, H., Singh, A., Kumar, R., 2020. Assessment methods of urban microclimate and its parameters: A critical review to take the research from lab to land. Urban Clim. 34, 100690. https://doi.org/10.1016/j.uclim.2020.100690.

Bolker, B.M., 2008. Ecological Models and Data in R. Princeton University Press. https://doi.org/10.1515/9781400840908.

Bonafoni, S., Baldinelli, G., Verducci, P., 2017. Sustainable strategies for smart cities: Analysis of the town development effect on surface urban heat island through remote sensing methodologies. Sustain. Cities Soc. 29, 211–218. https://doi.org/10.1016/j.scs.2016.11.005.

Bosch, M., Locatelli, M., Hamel, P., Remme, R.P., Chenal, J., Joost, S. (Eds.), 2021. A spatially explicit approach to simulate urban heat mitigation with InVEST (v3.8.0). Geosci. Model Dev. https://doi.org/10.5194/gmd-14-3521-2021.

Bowler, D.E., Buyung-Ali, L., Knight, T.M., Pullin, A.S., 2010. Urban greening to cool towns and cities: A systematic review of the empirical evidence. Landsc. Urban Plan. 97, 147–155. https://doi.org/10.1016/j.landurbplan.2010.05.006.

Broadbent, A.M., Coutts, A.M., Tapper, N.J., Demuzere, M., beringer, J., 2018. The microscale cooling effects of water sensitive urban design and irrigation in a suburban environment | Theoretical and Applied Climatology. Theor. Appl. Climatol.

Changnon, S.A., Kunkel, K.E., Reinke, B.C., 1996. Impacts and Responses to the 1995 Heat Wave: A Call to Action. Bull. Am. Meteorol. Soc. 77, 1497–1506. https://doi.org/10.1175/1520-0477(1996)077<1497:IARTTH>2.0.CO;2.

Congedo, L., 2021. Semi-Automatic Classification Plugin: A Python tool for the download and processing of remote sensing images in QGIS. J. Open Source Softw. 6 (64), 3172.

R Core team, 2022. R: The R Project for Statistical Computing [WWW Document]. URL https://www.r-project.org/ (accessed 1.1.24).

Crawley, M.J., 2012. The R Book. John Wiley & Sons.

Elliott, H., Eon, C., Breadsell, J.K., 2020. Improving city vitality through urban heat reduction with green infrastructure and design solutions: a systematic literature review. Buildings 10, 219. https://doi.org/10.3390/buildings10120219.

Estoque, R.C., Murayama, Y., 2017. Monitoring surface urban heat island formation in a tropical mountain city using Landsat data (1987–2015). ISPRS J. Photogramm. Remote Sens. 133, 18–29. https://doi.org/10.1016/j.isprsjprs.2017.09.008.

Freitas, S., Catita, C., Redweik, P., Brito, M.C., 2015. Modelling solar potential in the urban environment: State-of-the-art review. Renew. Sustain. Energy Rev. 41, 915–931. https://doi.org/10.1016/j.rser.2014.08.060.

Grizonnet, M., Michel, J., Poughon, V., Inglada, J., Savinaud, M., Cresson, R., 2017. Orfeo ToolBox: open source processing of remote sensing images. Open Geospatial Data Softw. Stand. 2, 15. https://doi.org/10.1186/s40965-017-0031-6.

Halder, B., Bandyopadhyay, J., Banik, P., 2021. Monitoring the effect of urban development on urban heat island based on remote sensing and geo-spatial approach in Kolkata and adjacent areas, India. Sustain. Cities Soc. 74, 103186.
Heaviside, C., Macintyre, H., Vardoulakis, S., 2017. The urban heat island: implications for health in a changing environment. Curr. Environ. Health Rep. 4, 296–305.
Hofierka, J., Gallay, M., Onačillová, K., Hofierka, J., 2020. Physically-based land surface temperature modeling in urban areas using a 3-D city model and multispectral satellite data. Urban Clim. 31, 100566. https://doi.org/10.1016/j.uclim.2019.100566.
Hondula, D.M., Barnett, A.G., 2014. Heat-related morbidity in brisbane, australia: spatial variation and area-level predictors. Environ. Health Perspect. 122, 831–836. https://doi.org/10.1289/ehp.1307496.
Hu, L., Wendel, J., 2019. Analysis of urban surface morphologic effects on diurnal thermal directional anisotropy. ISPRS J. Photogramm. Remote Sens. 148, 1–12. https://doi.org/10.1016/j.isprsjprs.2018.12.004.
Inglada, J., Vincent, A., Arias, M., Tardy, B., Morin, D., Rodes, I., 2017. Operational high resolution land cover map production at the country scale using satellite image time series. Remote Sens. 9, 95. https://doi.org/10.3390/rs9010095.
IPCC, 2023. Climate Change 2023: Synthesis Report. Contribution of Working Groups I, II and III to the Sixth Assessment Report of the Intergovernmental Panel on Climate Change IPCC, Geneva, Switzerland. H. Lee and J. Romero (eds.).
Johnson, M.T.J., Munshi-South, J., 2017. Evolution of life in urban environments. Science 358, eaam8327. https://doi.org/10.1126/science.aam8327.
Jones, L., Anderson, S., Læssøe, J., Banzhaf, E., Jensen, A., Bird, D.N., Miller, J., Hutchins, M.G., Yang, J., Garrett, J., Taylor, T., Wheeler, B.W., Lovell, R., Fletcher, D., Qu, Y., Vieno, M., Zandersen, M., 2022. A typology for urban Green Infrastructure to guide multifunctional planning of nature-based solutions. Nat.-Based Solut. 2, 100041. https://doi.org/10.1016/j.nbsj.2022.100041.
Kim, Y.-H., Baik, J.-J., 2002. Maximum urban heat island intensity in Seoul. J. Appl. Meteorol. Climatol. 41, 651–659. https://doi.org/10.1175/1520-0450(2002)041<0651:MUHIII>2.0.CO;2.
Kim, Y.-H., Baik, J.-J., 2005. Spatial and temporal structure of the urban heat island in Seoul. J. Appl. Meteorol. Climatol. 44, 591–605. https://doi.org/10.1175/JAM2226.1.
Konijnendijk, C.C., 2023. Evidence-based guidelines for greener, healthier, more resilient neighbourhoods: Introducing the 3–30–300 rule. J. For. Res. 34, 821–830. https://doi.org/10.1007/s11676-022-01523-z.
Liu, S., Zang, Z., Wang, W., Wu, Y., 2019. Spatial-temporal evolution of urban heat Island in Xi'an from 2006 to 2016. Phys Chem. Earth Parts ABC, Sensing and Sensor Systems for Urban Environmental Studies 110, 185–194. https://doi.org/10.1016/j.pce.2018.11.007.
Maxwell, S.L., Fuller, R.A., Brooks, T.M., Watson, J.E.M., 2016. Biodiversity: The ravages of guns, nets and bulldozers. Nature 536, 143–145. https://doi.org/10.1038/536143a.
Mohammad, P., Goswami, A., 2021. Quantifying diurnal and seasonal variation of surface urban heat island intensity and its associated determinants across different climatic zones over Indian cities. Giscience Remote Sens. 58, 955–981. https://doi.org/10.1080/15481603.2021.1940739.
Morin, É., 2022. Repenser la conception des corridors écologiques à travers l'espace et le temps : l'apport de la télédétection à très haute résolution spatiale (phdthesis). Université de Poitiers.
Morin, E., Herrault, P.-A., Guinard, Y., Grandjean, F., Bech, N., 2022. The promising combination of a remote sensing approach and landscape connectivity modelling at a fine scale in urban planning. Ecol. Indic. 139, 108930. https://doi.org/10.1016/j.ecolind.2022.108930.
Morin, E., Razafimbelo, N.T., Yengué, J.-L., Guinard, Y., Grandjean, F., Bech, N., 2024. Mapping past land cover on Poitiers in 1993 at very high resolution using GEOBIA approach and open data. Data Brief 52, 109829. https://doi.org/10.1016/j.dib.2023.109829.
Motazedian, A., Coutts, A.M., Tapper, N.J., 2020. The microclimatic interaction of a small urban park in central Melbourne with its surrounding urban environment during heat events. Urban for. Urban Green. 52, 126688. https://doi.org/10.1016/j.ufug.2020.126688.
Mueller, C., Hussain, R., Xian, G., Shi, H., Arab, S., 2023. Mapping The Surface Urban Heat Island Effect Using The Landsat Surface Temperature Product, in: IGARSS 2023 - 2023 IEEE International Geoscience and Remote Sensing Symposium. Presented at the IGARSS 2023 - 2023 IEEE International Geoscience and Remote Sensing Symposium, pp. 441–444. https://doi.org/10.1109/IGARSS52108.2023.10282386.
Mushore, T.D., Odindi, J., Dube, T., Mutanga, O., 2017. Prediction of future urban surface temperatures using medium resolution satellite data in Harare metropolitan city, Zimbabwe. Build. Environ. 122, 397–410. https://doi.org/10.1016/j.buildenv.2017.06.033.
Nieuwenhuijsen, M.J., Dadvand, P., Márquez, S., Bartoll, X., Barboza, E.P., Cirach, M., Borrell, C., Zijlema, W.L., 2022. The evaluation of the 3–30-300 green space rule and mental health. Environ. Res. 215, 114387. https://doi.org/10.1016/j.envres.2022.114387.
Norton, B.A., Coutts, A.M., Livesley, S.J., Harris, R.J., Hunter, A.M., Williams, N.S.G., 2015. Planning for cooler cities: A framework to prioritise green infrastructure to mitigate high temperatures in urban landscapes. Landsc. Urban Plan. 134, 127–138. https://doi.org/10.1016/j.landurbplan.2014.10.018.
Oke, T.R., 1976. The distinction between canopy and boundary-layer urban heat islands. Atmosphere 14, 268–277. https://doi.org/10.1080/00046973.1976.9648422.
Oke, T.R., Johnson, G.T., Steyn, D.G., Watson, I.D., 1991. Simulation of surface urban heat islands under 'ideal' conditions at night part 2: Diagnosis of causation. Bound.-Layer Meteorol. 56, 339–358. https://doi.org/10.1007/BF00119211.
Onačillová, K., Gallay, M., 2018. Spatio-TEMPORAL analysis of surface urban heat island based on landsat etm+ and oli/tirs imagery in the city of Košice, Slovakia. Carpathian J. Earth Environ. Sci. 13, 395–408.
Puissant, A., Rougier, S., Stumpf, A., 2014. Object-oriented mapping of urban trees using Random Forest classifiers. Int. J. Appl. Earth Obs. Geoinformation 26, 235–245. https://doi.org/10.1016/j.jag.2013.07.002.
Ramalho, C.E., Hobbs, R.J., 2012. Time for a change: dynamic urban ecology. Trends Ecol. Evol. 27, 179–188. https://doi.org/10.1016/j.tree.2011.10.008.
Ranagalage, M., Estoque, R.C., Murayama, Y., 2017. An Urban Heat Island Study of the Colombo Metropolitan Area, Sri Lanka, Based on Landsat Data (1997–2017). ISPRS Int. J. Geo-Inf. 6, 189. https://doi.org/10.3390/ijgi6070189.
Rouse, J., Haas, R., Schell, J., Deering, D., 1973. Monitoring vegetation systems in the great plains with erts.
Santamouris, M., Synnefa, A., Asssimakopoulos, M., Livada, I., Pavlou, K., Papaglastra, M., Gaitani, N., Kolokotsa, D., Assimakopoulos, V., 2008. Experimental investigation of the air flow and indoor carbon dioxide concentration in classrooms with intermittent natural ventilation. Energy Build. 40, 1833–1843. https://doi.org/10.1016/j.enbuild.2008.04.002.
Sharp, R., Douglass, J., Wolny, S., Arkema, K., Bernhardt, J., Bierbower, W., Chaumont, N., Denu, D., Fisher, D., Glowinski, K., 2020. InVEST 3.9. 0. post24+ ug. g66b919f User's Guide. Nat. Cap. Proj. Stanf. Univ. Univ. Minn. Nat. Conserv. World Wildl. Fund.
Shi, Y., Zhang, Y., 2018. Remote sensing retrieval of urban land surface temperature in hot-humid region. Urban Clim. 24, 299–310. https://doi.org/10.1016/j.uclim.2017.01.001.
Taha, H., 2004. Heat Islands and Energy, in: Cleveland, C.J. (Ed.), Encyclopedia of Energy. Elsevier, New York, pp. 133–143. https://doi.org/10.1016/B0-12-176480-X/00394-6.
Tieskens, K.F., Smith, I.A., Jimenez, R.B., Hutyra, L.R., Fabian, M.P., 2022. Mapping the gaps between cooling benefits of urban greenspace and population heat vulnerability. Sci. Total Environ. 845, 157283. https://doi.org/10.1016/j.scitotenv.2022.157283.
Tomlinson, C.J., Chapman, L., Thornes, J.E., Baker, C.J., 2012. Derivation of Birmingham's summer surface urban heat island from MODIS satellite images. Int. J. Climatol. 32, 214–224. https://doi.org/10.1002/joc.2261.
United Nations, 2018. 68% of the world population projected to live in urban areas by 2050, says UN | UN DESA | United Nations Department of Economic and Social Affairs [WWW Document]. URL https://www.un.org/development/desa/en/news/population/2018-revision-of-world-urbanization-prospects.html (accessed 11.28.23).
Wloczyk, C., Borg, E., Richter, R., Miegel, K., 2011. Estimation of instantaneous air temperature above vegetation and soil surfaces from Landsat 7 ETM+ data in northern Germany. Int. J. Remote Sens. 32, 9119–9136. https://doi.org/10.1080/01431161.2010.550332.
Wouters, H., De Ridder, K., Poelmans, L., Willems, P., Brouwers, J., Hosseinzadehtalaei, P., Tabari, H., Vanden Broucke, S., van Lipzig, N.P.M., Demuzere, M., 2017. Heat stress increase under climate change twice as large in cities as in rural areas: A study for a densely populated midlatitude maritime region. Geophys. Res. Lett. 44, 8997–9007. https://doi.org/10.1002/2017GL074889.
Yang, J., Wang, Y., Xiu, C., Xiao, X., Xia, J., Jin, C., 2020. Optimizing local climate zones to mitigate urban heat island effect in human settlements. J. Clean. Prod. 275, 123767.
ZAR, J., 2010. Biostatistical analysis, Prentice-Hall, New Jersey. ed.
Zawadzka, J.E., Harris, J.A., Corstanje, R., 2021. Assessment of heat mitigation capacity of urban greenspaces with the use of InVEST urban cooling model, verified with daytime land surface temperature data. Landsc. Urban Plan. 214, 104163. https://doi.org/10.1016/j.landurbplan.2021.104163.